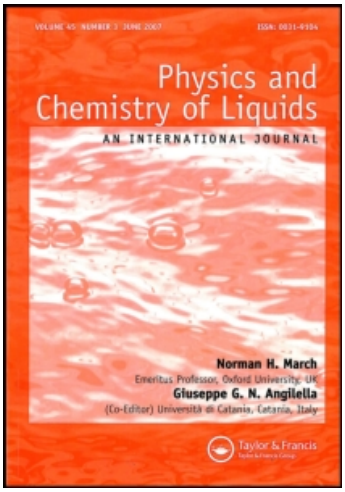

Physics and Chemistry of Liquids
Publication details, including instructions for authors and subscription information:
http://www.informaworld.com/smpp/title~content=t713646857

Density and Thermal Expansion of Molten Manganese, Iron, Nickel, Copper, Aluminum and Tin by Means of the Gamma-Ray Attenuation Technique

P. M. Nasch[ab]; S. G. Steinemann[a]
[a] Institute de Physique Expérimentale, Université de Lausanne, Lausanne-Dorigny, Switzerland [b] Mineral Physics Group, School of Ocean and Earth Science and Technology, University of Hawaii, Honolulu, HI, USA

To cite this Article Nasch, P. M. and Steinemann, S. G.(1995) 'Density and Thermal Expansion of Molten Manganese, Iron, Nickel, Copper, Aluminum and Tin by Means of the Gamma-Ray Attenuation Technique', Physics and Chemistry of Liquids, 29: 1, 43 — 58
To link to this Article: DOI: 10.1080/00319109508030263
URL: http://dx.doi.org/10.1080/00319109508030263

Phys. Chem. Liq., 1995, Vol. 29, pp. 43–58
Reprints available directly from the publisher
Photocopying permitted by license only

DENSITY AND THERMAL EXPANSION OF MOLTEN MANGANESE, IRON, NICKEL, COPPER, ALUMINUM AND TIN BY MEANS OF THE GAMMA-RAY ATTENUATION TECHNIQUE

P. M. NASCH† and S. G. STEINEMANN

Institut de Physique Expérimentale, Université de Lausanne, CH 1015 Lausanne-Dorigny, Switzerland

(Received 18 August 1994)

New experimental data for the density and the coefficient of thermal expansion of pure liquid Mn, Fe, Ni, Cu, Al and Sn at temperatures between melting and 1973K using the γ-ray attenuation technique are reported. An extensive study of sources of random and systematic errors has shown a maximum error of 0.75% in absolute density measurements. In the temperature range studied, the density behaves linearly with temperature. The density at the melting point and the coefficient of thermal expansion are in accordance with those of other studies. Comparison of the specific heat ratios γ calculated with the results of this study with those obtained using structural data from diffraction experiments shows large and even non-physical discrepancies, e.g., in the case of Mn. Solid-like viscoelastic behavior in the low-Q region is suggested as a possible cause of such anomaly while shear components would contribute noticeably to reduce the liquid compressibility. It is shown that expansivities of the present study are giving heat capacities at constant volume in the range 3R–4R which is in good accordance with theory predicting 3R as the ionic contribution and about 1R as the electronic contribution. Previously reported data for thermal expansion are giving a wider range of degrees of freedom.

KEY WORDS: γ-ray attenuation technique, specific heat ratio, bulk modulus.

1 INTRODUCTION

The knowledge of the density and the coefficient of thermal expansion of liquid is important for the discussion of thermodynamic properties. For example, the density and the thermal expansion give access to the compressibility, the specific heat ratio, the thermal pressure coefficient and other microscopic parameters, such as the packing fraction in the framework of the hard-sphere model. Basically, the thermodynamics of liquid involve the particle number density ρ_0, instead of the mass density ρ. Thus the Gamma-Attenuation Technique (hereafter referred to as GAT) is especially suitable. Indeed, the basic law of attenuation gives the number of transmitted (non-diffused) photons N by

$$N = N_0 \exp\{-\sigma \rho_0 x\} \tag{1}$$

†Present address: Mineral Physics Group, School of Ocean and Earth Science and Technology, University of Hawaii, HIG room 115, 2525 Correa Road, Honolulu, HI 96822 USA.

where N_0 is the number of incident photons, x the path length and σ the total scattering cross-section. Eq. (1) expresses the fact that photon diffusion is only controlled by the number density of atoms ρ_0 and that the mass is not involved.

Beside the methodological aspect, the use of the GAT appears to be advantageous at high temperatures, as already suggested by Drotning[1]. The gamma beam offers a probe which is neither in thermal nor in physical contact with the liquid, i.e. GAT is a *non-contacting method*. Since the free liquid surface is not involved in the measurement, several problems, such as sample volatilization, surface tension corrections, or surface oxide films, do not exist. This method, based on absorption of a penetrating beam, is considered by many, especially by Russian scientists[2-7], as the most reliable technique of density measurements of liquid metals and alloys. It has been quite extensively used on molten iron[1-5] but less for other high melting point materials. It also has exigencies, namely the need for non-reactive crucible materials and sophisticated radiation detection equipment. Furthermore, radiation protection rules must be followed. One usually writes the attenuation law of a beam of mono-energetic well-collimated radiation as

$$I(x) = I_0 \exp\{-\mu\rho x\} \tag{2}$$

where I_0 and $I(x)$ are the γ-flux intensities of the incident beam, and at the depth x inside the material respectively, μ is the mass attenuation (or absorption) coefficient, and ρ is the mass density. The mass attenuation coefficient μ is related to the total scattering cross-section σ by the relation $\mu = N_A\sigma/A$, and similarly, the mass density ρ is related to the number density ρ_0 by the expression $\rho = A\rho_0/N_A$, where N_A is Avogadro's number, and A the atomic mass.

As the temperature changes, the density and length also change; so Eq. (2) becomes

$$I(x, T) = I_0(T) \exp\{-\mu\rho(T)\, x(T)\} \tag{3}$$

2 EXPERIMENTAL PROCEDURE

The density of the material is determined from the attenuation which is produced by the passage of a collimated beam of mono-energetic γ radiation through the material, whose length and attenuation coefficient are independently determined. The GAT for density measurements has been previously described in detail by Drotning[1,8,9]. Here only some main features of our procedure are given.

2.1 High-temperature Assembly

The high-temperature setup is schematically represented in Figure 1. Samples with nominal purities of at least 99.98% were first prepared by casting in order to assure full density and good homogeneity. The metal sample is contained in an Al_2O_3 ceramic crucible (Metoxit) which has the required chemical inertness against molten refractive metals, as confirmed by microprobe analyses of the contact zone after the

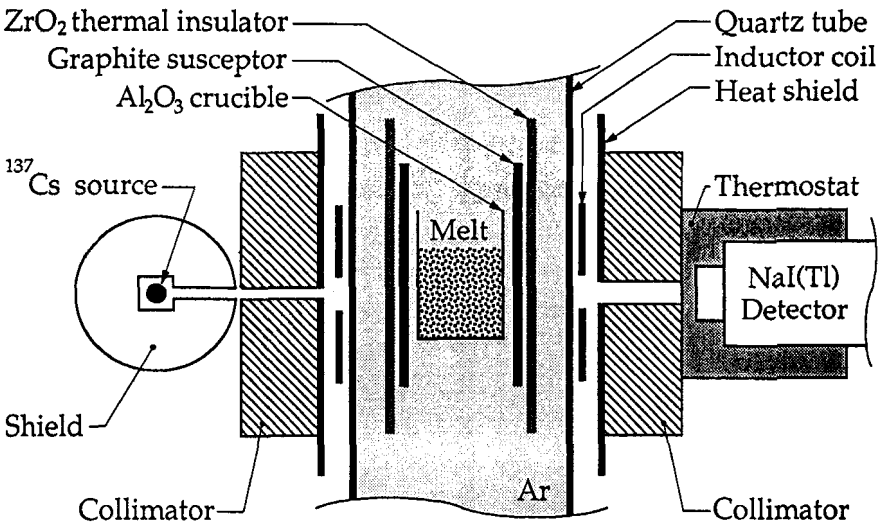

Figure 1 Schematic diagram of the high-temperature γ-ray attenuation experimental apparatus.

absorption experiment. The crucible is surrounded by a graphite sleeve susceptor which is coupled to the one-turn inductor coil of a 12 kW 700 kHz HF-generator (Plustherm). A 5-mm-thick ZrO_2 radiation shield (Zircar) serves for thermal insulation of the susceptor. The sample temperature is monitored by an alumina-sheathed Pt-Pt13%Rh (type-S) thermocouple positioned in the melt. The crucible is supported by a boron-nitride bar. The measuring assembly is contained in a 60 mm-diameter clear-fused quartz tube held by water-cooled flanges. The high-temperature chamber is evacuated with a high-vacuum system for the heating-up and melting. Then purified argon is introduced for the measurement cycle.

The γ-rays are produced by a Pb-shielded ^{137}Cs quasi-punctual source of 350 mCi nominal activity. The entry collimator has a diameter of 3 mm (100 mm length) and the exit collimator has a diameter of 12 mm (50 mm length) slightly bigger than the beam divergence. Alignment is obtained with a He-Ne laser beam and the entire collimator system is water-cooled to ascertain its stability.

2.2 Detector System

A block diagram of the detector system is shown in Figure 2. A temperature-controlled NaI(Tl) scintillator is coupled to a photomultiplier tube (Dumont 6292). Temperature control of the detector system is crucial for constant scintillator efficiency, black noise (thermoelectric effect), photomultiplier gain and spectral sensitivity. The calculated resolution of 8.2% and an experimentally determined value of 9% are in agreement with stated specifications (7%–9%). An amplifier with automatic gain stabilizer (Harshaw, model Na-23) ensures count-rate stability of the electronic counting system. Optimization of the electronic counting system resulted for a maximum count-rate threshold of 20,000 cps over the entire scintillator energy

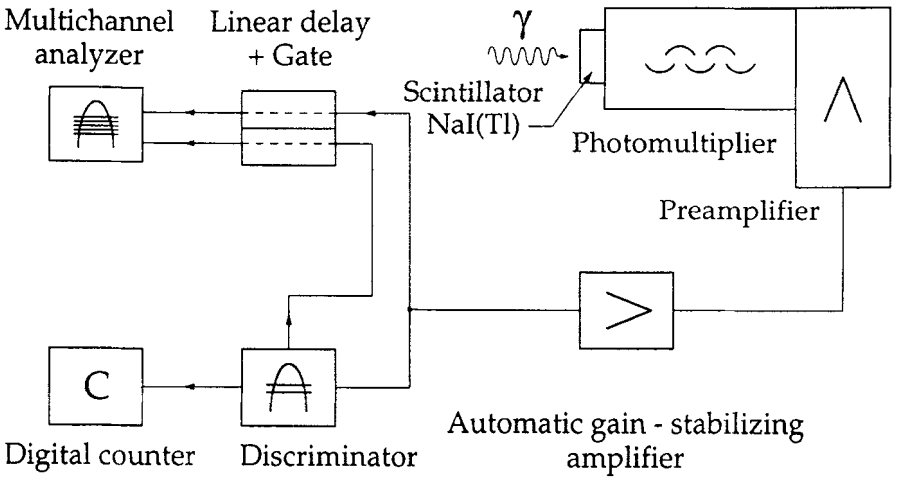

Figure 2 Block diagram of the γ-ray detector system.

spectrum. Above this limit, the linearity of the counting system is lost. At higher rates, absorbers must be placed into the γ-rays path to reduce the integral count-rate and ensure counting in the linear response region. A multichannel analyzer enables the adjustment of the discriminator in order to pass the entire ^{137}Cs photoelectric peak detected in the NaI(Tl) scintillator. The acquisition time always goes to 10^6 counts. All count-rates are corrected for the dead time τ of the electronic counting system, which has been experimentally determined by both the two-source and the two-absorber methods, and is 10 ± 1 μs.

3 PRELIMINARY CALIBRATIONS

The temperature dependence of $x(T)$ in Eq. (3) is simply given by the linear thermal expansion α_l of the crucible material

$$x(T) = \kappa D(T_0)[1 + \alpha_l(T - T_0)] \tag{4}$$

where $\alpha_l = 8.1 \times 10^{-6}\,K^{-1}$ as given by the manufacturer. κ is a dimensionless correction factor as discussed below, and D is the nominal diameter of the crucible at the reference temperature T_0. D is measured using a micrometer set always at the same height inside the crucible, and is averaged on 5 measurements.

The nominal path D, i.e. the crucible diameter is different from the average γ-ray path $\langle x \rangle$ owing to the cylindrical shape of the crucible and the finite extension of the γ-beam. Let $f(R, y)$ be a geometrical function describing the curvature of the crucible (Fig. 3), where $R = D/2$ is the crucible radius, and $g(r, y)$ a geometrical function describing the section of the γ-beam, where r is the γ-beam radius. Assuming a cylindrical symmetry for both the crucible and the beam, and neglecting flux

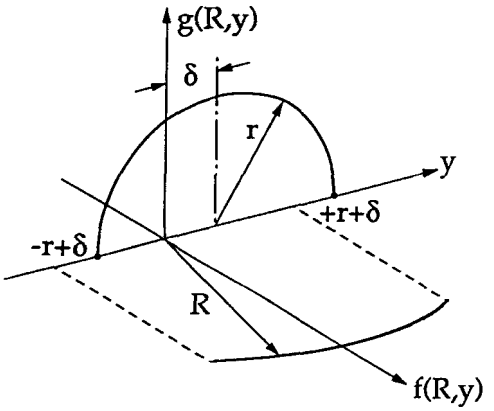

Figure 3 Geometrical configuration for the mean γ-ray path analysis.

conservation constraints, the geometrical average path can be written as a normalized weighted integral of the form

$$\langle x\rangle = 2\frac{\int_0^r f(R,y)\,g(r,y)dy}{\int_0^r g(r,y)dy} = 2\frac{\int_0^r \sqrt{R^2-y^2}\,\sqrt{r^2-y^2}\,dy}{\int_0^r \sqrt{r^2-y^2}\,dy} \tag{5}$$

The quality of the alignment (center of the beam to diameter of the crucible) can be accounted for by introducing an off-axis parameter δ in Eq. (5) as follow

$$\langle x\rangle = 2\frac{\int_{-r+\delta}^{r+\delta} f(R,y)\,g(r,y-\delta)dy}{\int_{-r+\delta}^{r+\delta} g(r,y-\delta)dy} = 2\frac{\int_{-r+\delta}^{r+\delta} \sqrt{R^2-y^2}\,\sqrt{r^2-(y-\delta)^2}\,dy}{\int_{-r+\delta}^{r+\delta} \sqrt{r^2-(y-\delta)^2}\,dy} \tag{6}$$

The correction factor κ is defined as the ratio $\langle x\rangle/D$. A numerical integration of Eq. (6) using typical values for $R = D/2$ of 13.1 mm and $r = 2.3 \pm 0.3$ mm (measured on a 12 h. exposure X-ray film) allows κ to be plotted with respect to incremental δ (Fig. 4). Misalignment is expected when loading the crucible into the high-temperature furnace. The effect of δ is treated as an error on a representative κ, chosen in assuming neither a perfect alignment ($\delta = 0$), nor an off-axis displacement greater than 1 mm. Under these conditions, $\kappa = 0.994 \pm 0.002$ (0.2%), which means that κ reduces D by 0.6% in our geometry. Fe, Ni and Al data were corrected using this value for κ (cylindrical crucible). In the case of Mn, Cu and Sn, κ is set equal to 1 because the crucibles used have two flat parallel portions (in this case $f(R, y)$ is constant and equal to R). It can be shown that the effect of temperature on κ through the crucible expansion (i.e. $R = R(T)$) and collimators expansion (i.e. $r = r(T)$) is negligible.

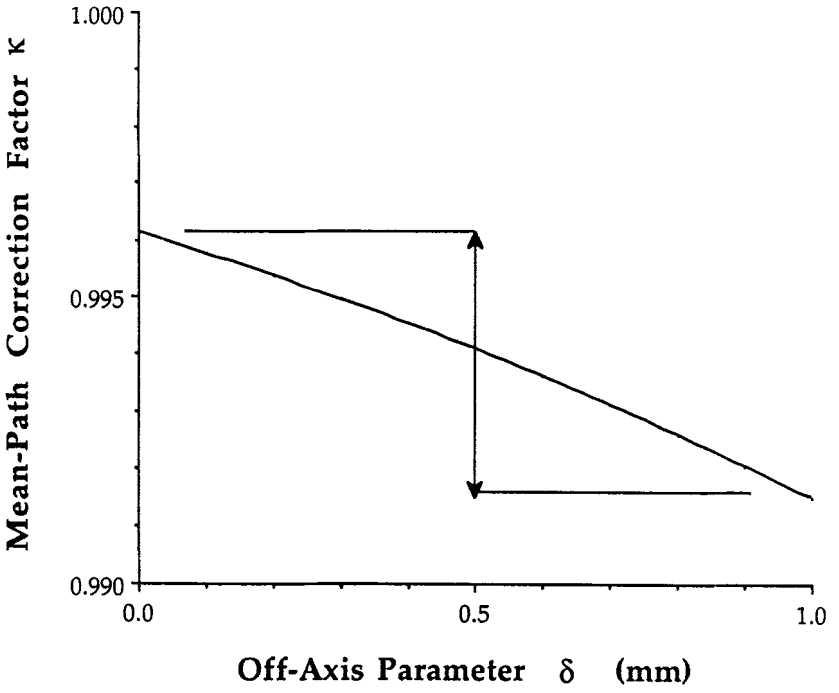

Figure 4 Dimensionless geometrical factor κ for correction of the γ-ray path versus off-axis misalignment parameter δ. Arrows show the range of uncertainty on κ associated with a misalignment parameter arbitrary set at $\delta = 0.5$ mm.

The temperature dependence of $I_0(T)$ in Eq. (3) is caused by the expansion of the different parts of the furnace; to first order it is

$$I_0(T) = I_0(T_0)[1 + \lambda(T - T_0)] \tag{7}$$

where λ corrects for the overall change in density with temperature of the quartz tube, the ZrO_2 insulation, the graphite susceptor, the Al_2O_3 crucible as well as the argon atmosphere. λ is experimentally determined, and amounts to $\lambda = (6.5 \pm 1.0) \times 10^{-6} K^{-1}$. This is the average value over 6 different runs (i.e. with different crucibles) and is supported by a theoretical estimation[1].

The mass attenuation coefficient $\mu(E, Z)$ is independent of the physical state of the sample, and is in particular temperature independent. However, since μ is geometry-dependent (because of non-ideal collimation), it is necessary to measure μ in situ for each separate material. For the purpose, a high precision step-shaped sample for Fe, Ni, Cu, Al and Sn has been prepared (Fig. 5), and has been machined out of the same cast as for high temperature run. By monitoring the transmitted amplitude $I(x)$ on a chart recorder while moving continuously the step-shaped sample up and down allows precise positioning of the γ-rays beam in the center of each step of known thickness x_i. For each step i, $I(x_i)$ is measured and the product $\mu\rho$, i.e. the *linear* attenuation coefficient, is computed using Eq. (2). δ is taken as X-ray density as obtained from powder (calibrated with Si).

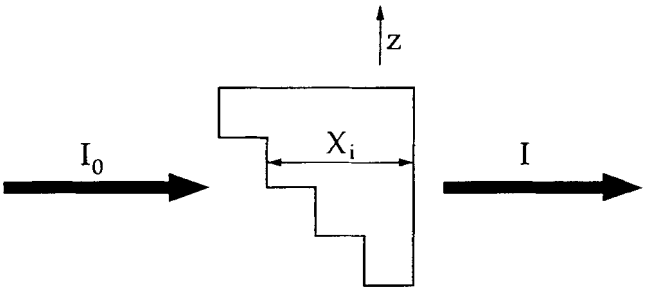

Figure 5 Sample shape for linear absorption coefficient measurement.

Our results for the mass attenuation coefficient μ are in good accord with some theoretical calculations (Tab. 1), which confirm that conditions of adequate geometry of collimating have been met and the measurement circuits has been properly tuned. By the propagation of random errors we have estimated a resulting error of 0.6% on μ measurements. This resulting error includes those made in the solid metal X-ray density measurement.

We have not been successful in making a massive Mn sample without cracks (by casting or by grinding thin plates of electrodeposited metal) and thus do not have a reliable measurement of μ for Mn. For this reason, the Mn mass attenuation coefficient at 0.662 MeV has been deduced from the linear variation of the diffusion total cross-section σ with the atomic number Z (Fig. 6). For small Z and an energy of 0.662 MeV, the scattering is dominated by the Compton effect[10]. But the photoelectric contribution (σ_{photo}) to σ becomes non-negligible at high atomic number as this is the case for Sn where it amounts to about 10% of the total cross-section. For Al, Fe, Ni and Cu, σ_{photo} does not exceed the uncertainty associated with measurements of σ (0.6%) (Tab. 1). The total cross-section σ as obtained from our in situ measurements with respect to the atomic number Z is plotted in Figure 6. After subtraction of the Sn photoelectric contribution, the curve displays the expected linear variation which

Table 1 Measured and calculated mass attenuation coefficient μ.

Metals	Z	$\mu\ (cm^2\ g^{-1})$		$\sigma\ (\times 10^{-24}\ cm^2)$	
		This work	*Tabulated*[a]	*Total*	*Photoelectric*[a]
Al	13	0.0747	0.0749	3.35	0.0029
Mn[b]	25	0.072	—	6.56	—
Fe	26	0.0734	0.0733	6.81	0.0754
Ni	28	0.0755	—	7.36	—
Cu	29	0.0711	0.0722	7.50	—
Sn	50	0.0746	0.0748	14.70	1.455

[a] From reference 10
[b] Interpolated value (see text for details)

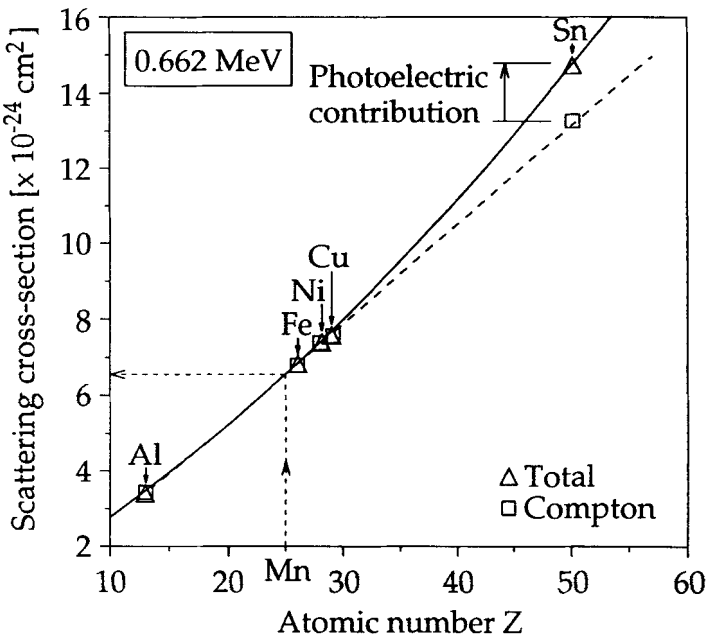

Figure 6 Dependence at 0.662 MeV of the total scattering cross-section σ with the atomic number Z (full line). When the photoelectric contribution is substracted, especially at high Z, the resulting cross-section varies linearly with Z (dashed line). The Compton effect dominates the processes of diffusion. The Mn mass attenuation coefficient is interpolated from the linear fit.

allows the mass attenuation coefficient for Mn to be interpolated. This procedure gives a value for μ of $0.072\,cm^2\,g^{-1}$ with a rms deviation of $\pm 0.002\,cm^2\,g^{-1}$ (3%).

4 ERRORS

A detailed analysis of our experiment has be done through an extensive study of random and systematic errors. Using the standard formulation for the propagation of random errors[8,11] an upper limit of 0.75% as the highest possible error of the absolute density is found. It results essentially from the uncertainty in the mass attenuation coefficient μ(0.6%), the dead time τ(10%) and the corrected path length inside the sample (0.4% or 0.2% when using square crucibles). This calculated error was tested by repeating experiments up to 2 times, with differences in the density at the melting point ρ_{mp} being smaller than 0.8%. The overall error associated with the Gamma Attenuation Technique reported in the literature is in the range of 0.2%[8] up to 2.7%[12]. In our geometry, the lower limit of the errors is 0.11% when only the stochastic behaviour of the nuclear disintegration is taken into account. A numerical example, similar to that reported by Drotning[8], illustrates the analysis and is presented in Table 2. For further details on the error analysis, the reader can refer in the literature to those works of Drotning[1,8] and Gardner *et al.*[11]

Table 2 Resultant percentage error in the density for three sets of uncertainties in the input data parameters. Numerical values are taken from a nickel run.

Parameter	*Input data*	*Percentage Standard Deviation*		
		Set A	*Set B*	*Set C*
$R_0(T)$[a]	5741 [cps]	0.1 (0.48)[b]		
$R(T)$	1308 [cps]	0.1 (0.44)		
τ	10 [μs]	10 (8.40)		0
μ	0.0755 [cm^2g^{-1}]	0.6 (36.0)	0.1[c]	0.05[e]
κ	0.994	0.2 (4.00)	0.0[d]	0.0
$D(T_0)$	2.632 [cm]	0.2 (4.00)		0.0
T_0	298 [K]	1.0		0.0
T	1973 [K]	1.0 (2.92)		0.0
λ	6×10^{-6} [K^{-1}]	20		0.0
α_l	8.1×10^{-6} [K^{-1}]	20		0.0
$\rho(T)$	7.67 [g cm^{-3}]	±0.75%	±0.42%	±0.11%

[a] R_0 and R are measured count-rates non-corrected from the dead time losses
[b] Numbers in parentheses denote the variance contribution ($\times 10^{-6}$)
[c] Experimental error from statistical distribution of several independent measurements
[d] Using a crucible with two flat parallel sections cancels the κ-correction and its associated error
[e] Inherent statistical error (stochastic) in in-situ measurements of μ by γ-ray densimetry

5 RESULTS

Density data points have been obtained for Mn, Fe, Ni, Cu, Al and Sn in the temperature range from their respective melting points to a maximum temperature of 1973 K, and this when measuring with increasing or decreasing temperatures. The least-squares fits to the data of the density as a function of temperature over the range studied have shown that, except for tin, it is suitable to limit the polynomial development of the density to the first order, i.e.

$$\rho(T) = a + b(T - T_{mp}) \tag{8}$$

where $a = \rho_{mp}$ is the density at the melting point T_{mp} and $b = (d\rho/dT)_P$. The coefficient of thermal expansion α is then calculated as the ratio $-b/a$. In the case of tin, a quadratic least-squares fit is found to be appropriate for the large temperature range investigated (1500°C). Then Eq. (8) becomes

$$\rho(T) = a + b(T - T_{mp}) + c(T - T_{mp})^2 \tag{9}$$

We present in Table 3 our results of the density at the melting point ρ_{mp} and coefficients b ane c. The density at the melting point is, within the stated experimental errors, in close agreement with previous measurements. Table 4 summarizes results for the coefficient of thermal expansion α (see Tables 3 and 4 for detailed references). Comparison is made with results obtained using the Gamma Attenuation Technique and the conventional methods (e.g. Archimedean, maximum bubble

Table 3 Measured density at the melting point ρ_{mp} and temperature coefficients b and c.

	Mn	*Fe*	*Ni*	*Cu*	*Al*	*Sn*	
T range (K)	1518–1866	1809–1953	1726–1973	1356–1900	933–1613	505–1503	
						Eq. (8)	Eq. (9)
ρ_{mp} (g cm^{-3})	5.95	6.98	7.81	8.02	2.375	6.99	7.02
b ($\times 10^{-4}$ g cm^{-3} K^{-1})	−10.53	−5.72	−7.26	−6.09	−2.33	−6.01	−7.77
c ($\times 10^{-7}$ g cm^{-3} K^{-2})	–	–	–	–	–	–	1.03
Literature:							
ρ_{mp} (g cm^{-3}) GAT	–	7.015–7.078[a]	7.85[b]	7.893–8.019[c]	2.39[d]	6.962–6.991[e]	
ρ_{mp} (g cm^{-3}) CM	5.38–6.43[f]	6.96–7.24[g]	7.75–8.03[g]	7.86–8.09[g]	2.37–2.41[g]	6.93–7.00[g]	

[a] From Refs. 1, 2–5 [b] From Ref. 1 [c] From Refs. 1, 3 [d] From Refs. 9, 13–15 [e] From Refs. 6, 9
[f] From Refs. 17–19 [g] From Refs. 17–22

Table 4 Coefficient of thermal expansion α ($\times 10^{-6}$ K^{-1}) obtained with the γ-attenuation technique (GAT) and compared with the results from conventional methods (CM).

Metal	*GAT*			*CM*	
	This work	*Others*	*Refs.*	*Range*	*Refs.*
Sc	–	~25[†]-57[§]	(6)	201	(7)
Ti	–	–		55–170	(17, 19)
V	–	–		60	(19)
Cr	–	140 ± 20[†]-307[§]	(6)	115–175	(17, 19)
Mn	177 ± 8	–		161–168	(17, 19)
Fe	82 ± 8	88–100	(1–4)	89–136	(17–21)
Co	–	91	(1)	93–157	(17, 19–21)
Ni	93 ± 3	94	(1)	82–147	(17–21)
Cu	76 ± 4	91–99	(1, 3)	84–119	(17, 20–22)
Zn	–	–		111–172	(17, 22)
Al	98 ± 5	102–119	(9, 13–15)	115–165	(17, 22)
Sn[*]	86 ± 2	93–94	(9, 16)	87–107	(17, 20–22)
[**]	111	110	(9)	–	

[†] estimated from figures [*] Linear fit (Eq. 8)
[§] estimated from data [**] Quadratic fit (Eq. 9)

pressure, dilatometric, pycnometric, liquid drop, etc.). Unlike the GAT, which is working at constant volume, the latter methods are all working at constant mass. It is for this reason precisely that they will be referred to hereafter as Constant Mass (CM). It is noted that GAT expansivities are in most case lower than those obtained with CM. Until now and among other things, this disparity has been attributed[1] to improved measurement techniques, technology and sample purity through the last three decades as well as the possibility that some critical corrections, such as surface tension and viscosity, have been underestimated in the CM. It could be added that an effect of wetting on α is likely to be less important for GAT than for CM where the entire metal-crucible interface is involved. In GAT experiments, it may be possible that metal vapors condense onto the quartz tube enclosure what leads to surestimate α. In any case apparently preference should be given to lower α values.

6 DISCUSSION

The expansivities obtained by GAT differ apparently from those obtained with classical methods. For the latter, the coefficient of thermal expansion is commonly associated with the temperature coefficient of the (mass) density, i.e. $\alpha = -1/\rho(d\rho/dT)_P$. According to Table 4, α(GAT) ≈ 0.8 α(CM), except for Mn. Thus, in view of the strong (square) contribution of α to the specific heat at constant volume C_V (see Eq. 12a below), a wider range of the degrees of freedom is resulting when α(CM) values are used. For example, using C_P data from Kubaschewski and Alcock[23], C_V ranges from 2.7 R to 4.3 R for the five metals under the present investigation, and is between 3.2 R and 4.1 R when α (GAT) values are used. This latter range is in better agreement with results for C_V in liquid simple metals where C_V is near 3 R[24]. For transition metals, and on physical ground, $C_V \approx 4R$ is expected, where 3 R is the ionic contribution and 1 R is the electronic contribution[24-26].

The coefficient of thermal expansion is defined by[27]

$$\alpha \equiv \frac{1}{\Omega}\left(\frac{\partial \Omega}{\partial T}\right)_P = \frac{1}{V}\left(\frac{\partial V}{\partial T}\right)_{P,N} \tag{10}$$

where Ω is the molar volume. It is the fractional increase in the volume per unit increase in temperature of a system maintained at constant pressure and constant mole number. The gamma-attenuation technique is certainly the perfect use of this definition; it measures the number of mole for a fixed volume whose limit is not and does not coincide with a free surface. The conventional methods on the other hand "measure" a new volume and new surface area, with changing configuration, image forces and other interactions.

Using a Maxwell relation, the thermal expansion can also be written as

$$\alpha = \left(\frac{\partial(\ln V)}{\partial T}\right)_P = \frac{1}{K_T}\left(\frac{\partial S}{\partial V}\right)_T = \frac{1}{K_T}\left(\frac{\partial P}{\partial T}\right)_V \tag{11}$$

which states that the volume will change with changing temperature to minimize the Gibbs free energy, the amount of the change being partly controlled by the elastic response of the medium[28]. The entropy term makes an important connection with temperature effects upon liquid structure; it measures an entropy change for which Cusack[29] observes "expansion reorganizes the short-range order, it does not merely increase the interatomic distances as it would in crystal". In fact, $(\partial S/\partial V)_T$ has the two contributions of a change in coordination number and of a change in average interatomic distance. An explicit form of these two contributions is not the same nor can be admitted that the two contributions are simply connected. Diffraction experiments only can give insight for such processes and Ocken and Wagner[30] show in the case of indium that both the interatomic distance and the coordination number decrease with increasing temperature. The latter contribution being dominant, the sign of $(\partial S/\partial V)_T$, which determines the sign of the expansion coefficient, becomes

positive as in "normal" materials. In fact, a reduction of the number of 1st neighbours has the effect to increase the attractive potential of the ions, and thus to reduce an average distance between ions.

Specific heat ratio at the melting point, i.e.

$$\gamma^{th} \equiv \frac{C_P}{C_V} = \frac{K_S}{K_T^{th}} = 1 + \frac{T_{mp}\alpha^2 K_S}{\rho_{mp} C_P} \tag{12a}$$

from thermodynamics, and the alternative formulation

$$\gamma^{st} \equiv \frac{C_P}{C_V} = \frac{K_S}{K_T^{st}} = \left(\frac{c_s}{c_0}\right)^2 S(0) \tag{12b}$$

from structure analysis are compared in Table 5. $K_S = \rho c_s^2$ is the adiabatic bulk modulus, c_s the sound velocity, $c_0 = \sqrt{RT_{mp}/A}$ the thermal velocity and $S(0) = \lim_{Q \to 0} S(Q)$, the long-wavelength limit of the structure factor. K_T^{st} is the isothermal bulk modulus taken from x-ray structure data and the well-known relation

$$S(0) = \rho_0 k_B T \frac{1}{K_T^{st}} \tag{13}$$

The ratios (12a) and (12b) are equal only for 2, or 3 metals. Differences are marked for Al and Sn, as already noticed[43], and Mn even shows a non-physical value $\gamma^{st} < 1$. Figure 7 displays the two ratios (12a) and (12b) when extended throughout the entire 3d series. Numerical values are easily obtained from the various thermodynamic properties computed in Table 6 (see references therein). The origin of the difference between γ^{th} and γ^{st} is not clearly understood at the present time. Waseda[43] refers on the work of Egami and Srolovitz[44] who suggested that atomic level stresses in disordered system could induce differences between the microscopic compressibility (related to local number and volume fluctuations) and the macroscopic (average) isothermal compressibility. However, attention should be

Table 5 Specific heat ratio (γ) [Eq. 12a] calculated using density and expansivity data from this work. The specific heat at constant pressure (C_P) and the sound velocity (c_S) are average values over selected data cited in refs. 23, 31–34 and refs. 34–41, respectively. Rms deviations on mean C_P and c_S introduce an error on γ not greater than 5%. Comparison is made with γ obtained from structure factor [Eqs. 12b, 13], where experimental data for $S(0)$ were taken from Waseda and Ueno[42].

	Mn	*Fe*	*Ni*	*Cu*	*Al*	*Sn*
T_{mp} (K)	1518	1809	1726	1356	933	505
c_S at mp (ms^{-1})	2442	3939	4033	3452	4705	2466
$c_0 = \sqrt{RT/A}$ at mp (ms^{-1})	479	519	494	421	536	188
$S(0)$	0.024	0.020	0.020	0.018	0.019	0.0098
$C_P/(N_A k_B)$	5.53	5.03	4.63	3.77	3.82	4.17
γ | thermodynamics	1.34	1.24	1.35	1.19	1.17	1.09
γ | structure	0.62	1.15	1.33	1.21	1.46	1.72

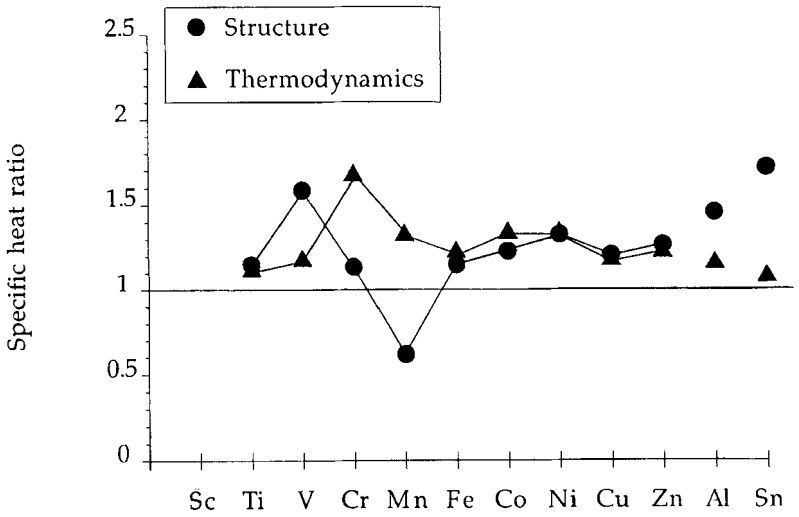

Figure 7 Specific heat ratios from thermodynamics [Eq. 12a] and from structure factor [Eq. 12b] for liquid 3d transition metals, along with values for Al and Sn.

focused on the following arguments. Molecular dynamic (MD) calculations on liquid alkali metals[45] clearly show viscoelastic behaviour persisting at low wavenumber Q. Furthermore, a high-resolution inelastic coherent neutron-scattering experiment[46] on liquid cesium and liquid rubidium near the melting point has given conclusive evidences that high-frequency collective modes can propagate in a similar fashion as collisionless zero-sound in a low (and restricted) Q region. Above the hydrodynamic limit $\omega\tau_S \gg 1$ with τ_S the Maxwell relaxation time for shear stress in the liquid, both high-frequency bulk K_∞ and shear modulus G_∞ of the liquid are involved in a high-frequency sound mode c_∞, as in solid. The effect of this solid-like elastic component in the low Q region is expected to reduce the local compressibility compared to the case $Q = 0$ where only the pure adiabatic longitudinal sound mode (pressure fluctuation) propagates. As a matter of fact, an anomalous γ has been also reported for cesium[43]. The shear relaxation time τ_S, defining a transition from pure adiabatic sound c (i.e. first sound and $\omega\tau_S \ll 1$) to zero-sound c_∞ ($\omega\tau_S \gg 1$), can be calculated using the Maxwell relation $\tau_S = \eta_S/G_\infty$ where η_S is the shear viscosity. In the low Q limit, G_∞ can be evaluated by means of Eq. (9) in Ref. 46 provided a reliable Einstein frequency ω_E can be found. Unfortunately, evaluating τ_S is actually of not much relevance in our discussion because, to the best of our knowledge, excitation energies of the collective modes (i.e. $\hbar\omega(Q)$) for high melting point liquid metals are still lacking, as these are obtained from dispersion relation. Consequently, Brillouin scattering experiments and MD calculations on these materials (especially Mn) are thus badly needed as these are the only techniques allowing characterization of the range of wavelength in which the liquid can sustain propagating collective excitation of both transverse and longitudinal type.

Finally, Table 6 summarizes various important thermodynamic properties for liquid 3d metals such as bulk moduli, Grüneisen parameter and thermal pressure

Table 6 Molar volume (Ω), adiabatic (K_S) and isothermal (K_T) bulk moduli, Grüneisen parameter (γ_G), and thermal pressure coefficient ($(\partial P/\partial T)_V$) at the melting point. Thermodynamic properties for Mn, Fe, Ni, Cu, Al and Sn are derived using density and expansivity data from this work. Density and expansivity data are from Kononenko *et al.*,[7] for Sc, from Saito *et al.*,[19] for Ti, V, Cr and Co, and from Crawley[22] for Zn. The specific heat at constant pressure (C_P, in $kJK^{-1}kg^{-1}$) and the sound velocity (c_S) are average values over selected data cited in refs. 23, 31–34 and refs. 34–41, respectively. K_T^{st} is computed using $S(0)$ data reported by Waseda and Ueno[42].

	Sc	*Ti*	*V*	*Cr*	*Mn*	*Fe*	*Co*	*Ni*	*Cu*	*Zn*	*Al*	*Sn*
$\Omega\,(cm^3\,mol^{-1})$	16.06	11.57	9.49	8.27	9.23	8.00	7.61	7.51	7.93	9.98	11.36	16.98
$K_S = \rho c_s^2$ (GPa)	–	80	121	116	35	108	125	127	95	53	53	43
$K_T^{th} = K_S/\gamma^{th}$ (GPa)	–	71	101	69	27	87	93	94	81	42	45	39
$K_T^{st} = \rho_0 k_B T_{mp}/S(0)$ (GPa)	26	70	76	102	57	94	101	96	79	41	36	25
$\gamma_G = \Omega\alpha K_S/AC_P$	–	1.2	1.5	2.8	1.3	1.6	2.2	2.2	1.8	2.4	1.9	2.2
$(\partial P/\partial T)_V = \alpha K_T^{th}\,(MPaK^{-1})$	–	3.9	6.1	7.9	4.7	7.2	8.4	8.7	6.1	6.1	4.4	3.3

coefficient according to Eq. (11). Results were computed with own data for the density and the coefficient of thermal expansion for the five metals investigated in this work and with data from other reports (see Table 6 for references) for the remaining metals of the 3d series. It can be seen from Table 6 that the variation of the cohesive properties, namely the molar volume and the bulk moduli, through the filling of the *d*-band has a pronounced anomaly – in the sense defined by Steinemann and Kéita[26] – in the middle of the *d* band. This anomalous behavior in liquid 3d transition metals has been interpreted by Steinemann and Kéita[26] as being due to magnetic excitations in the form of disordered local magnetic moments deriving from itinerant electron states and persisting well above the Curie temperature. Further on, the Grüneisen parameter, which characterizes the microscopic energetics ($\gamma_G \propto (\partial P/\partial U)_V$) (see Wallace[47]), shows strong values for chromium and zinc compared to the other metals within the series. Because this fact could simply result from overestimated thermal expansion values, really precise thermal expansion coefficient measurements, as obtained with the γ-ray attenuation technique, are needed on these materials.

Acknowledgement

We gratefully thank Ph. Renaud for helpful advise on the experimental procedure. This work was supported by the Swiss National Science Foundation.

References

1. W. D. Drotning, *High Temperatures-High Pressures*, **13**, 444 (1981).
2. Yu. N. Karmalin, G. F. Stasyuk, M. I. Gladkov, V. M. Bagin, L. S. Etelis and O. B. Borovskii, *Ind. Lab. USSR* (Translation), **39**, 739 (1973).
3. V. I. Yavoyskiy, A. A. Ezhov, V. F. Kravchenko, V. S. Uskov, Yu. I. Nebosov, Yu. A. Chernov and G. A. Dorofeyev, *Russ. Metall.*, **4**, 44 (1974).
4. A. S. Basin, Ya. L. Kolotov and S. V. Stankus, *High Temperatures-High Pressures*, **11**, 465 (1979).
5. G. V. Tyagunov, P. S. Popel', N. S. Kosilov, B. A. Baum and E. A. Klimenkov, *Russ. Metall.*, **5**, 44 (1981).
6. V. V. Makeer and P. S. Popel', *High Temperatures*, **28**, 525 (1990).
7. V. I. Kononenko, A. L. Sukhman, S. L. Gruverman and V. V. Torokin, *Phys. Stat. Sol. (a)*, **84**, 423 (1984).
8. W. D. Drotning, in *Thermal Expansion*, Ed. I. A. Peggs, Herausgeber (Plenum Press, New York, 1978) pp. 83–96.
9. W. D. Drotning, *High Temperature Sciences*, **11**, 265 (1979).
10. C. M. Davisson, in *Alpha-, Beta- and Gamma-Ray Spectroscopy*, Ed. K. Siegbahn (North-Holland Publishing Co., Amsterdam-London, 1974), vol. **1**, pp. 37–78 and pp. 827–843.
11. W. H. Gardner, G. S. Campbell and C. Calissendorff, *Soil Sci. Soc. Amer. Proc.*, **36**, 393 (1972).
12. T. Ishiguro, S. Tamaki and Y. Waseda, *J. Mat. Sci. Letters*, **3**, 875 (1984).
13. N. M. Kéita, P. Collet and S. G. Steinemann, *Helv. Phys. Acta*, **50**, 612 (1977).
14. N. M. Kéita, PhD Thesis, University of Lausanne, Switzerland (1977).
15. N. M. Kéita and S. G. Steinemann, *J. Phys. C: Solid State Phys.*, **11**, 4635 (1978).
16. G. Döge, *Z. Naturforschg.*, **21a**, 266 (1966).
17. *Handbook of Chemistry and Physics 1989–1990*, 70th edition, Ed. R. C. Weast (CRC Press, Boca Raton, Florida, 1989).
18. A. V. Grosse and A. D. Kirshenbaum, *J. Inorg. Nucl. Chem.*, **25**, 331 (1963).
19. T. Saito, Y. Shiraishi and Y. Sakuma, *Trans. Iron Steel Inst. Japan (ISIJ)*, **9**, 118 (1969).
20. L.-D. Lucas, *Mém. Scient. Rev. Mét.*, **69**, 395 (1972).
21. L.-D. Lucas, *Mém. Scient. Rev. Mét.*, **69**, 479 (1972).
22. A. F. Crawley, *Int. Metall. Rev.*, **19**, 32 (1974).

23. O. Kubaschewski and C. B. Alcock, *Metallurgical Thermochemistry*, Vol. 24 of the International Series on Materials Science and Technology, 5th edition, Ed. G. V. Raynor (Pergamon Press, New York, 1979).
24. P. Bratby, T. Gaskell and N. H. March, *Phys. Chem. Liq.*, **2**, 53 (1970).
25. I. Yokoyama, I. Ohkoshi and T. Satoh, *J. Phys. F*, **13**, 729 (1983).
26. S. G. Steinemann and N. M. Kéita, *Helv. Phys. Acta*, **61**, 557 (1988).
27. H. B. Callen, *Thermodynamics and an Introduction to Thermostatics* (John Wiley and Sons, New York, 1985), 2nd edition, p. 84.
28. G. K. White, *Contemporary Physics*, **34**, 193 (1993).
29. N. E. Cusack, *The Physics of Structurally Disordered Matter – An Introduction*, in Graduate Students Series in Physics, Ed. D. F. Brewer (Adam Hilger, Bristol, 1987), p. 68.
30. H. Ocken and C. N. J. Wagner, *Phys. Rev.*, **149**, 122 (1966).
31. R. Hultgren, P. D. Desai, D. T. Hawkins, M. Gleiser, K. K. Kelley and D. D. Wagman, *Selected Values of the Thermodynamic Properties of the Elements*, Ed. American Society for Metals (Metals Park, Ohio, 1973).
32. I. Barin, O. Knacke and O. Kubascheweski, *Thermochemical Properties of Inorganic Substances* (supplement), (Springer-Verlag Berlin, 1977).
33. S. Tamaki and Y. Waseda, *J. Phys. F*, **6**, L89 (1976).
34. T. Iida and R. I. L. Guthrie, *The Physical Properties of Liquid Metals*, Oxford Science Publications (Clarendon Press, Oxford 1988).
35. G. M. B. Webber and R. W. B. Stephens, in *Physical Acoustics: Principles and Methods*, Vol. IV (B), Ed. W. P. Mason (Academic Press, New York, 1968) Chap. 11, p. 53.
36. I. Yokoyama, I. Ohkoshi, Y. Waseda and W. H. Young, *Phys. Chem. Liq.*, **11**, 277 (1982).
37. R. Turner, E. D. Crozier and J. F. Cochran, *Canadian J. Phys.*, **50**, 2735 (1972).
38. H. J. Seemann and F. K. Klein, *Z. Angew. Phys.*, **19**, 368 (1965).
39. R. T. Beyer and E. M. Ring, in *Liquid Metals, Chemistry and Physics*, Ed. S. Z. Beer (Dekker, New York, 1972) pp. 431–460.
40. P. M. Nasch, M. H. Manghnani and R. A. Secco, *J. Geophys. Res.*, **99**, 4285 (1994).
41. N. M. Kéita, H. Morita and S. G. Steinemann, *Proc. 4th Int. Conf. on Rapidly Quenched Metals* (Sendai), 119 (1981).
42. Y. Waseda and S. Ueno, *Sci. Rep. RITU*, A-Vol. **34**, 15 (1988).
43. Y. Waseda, *Z. Naturforsch.*, **38a**, 509 (1983).
44. T. Egami and D. Srolovitz, *J. Phys. F*, **12**, 2141 (1982).
45. G. Jacucci and I. R. McDonald, *Molecular Physics*, **39**, 515 (1980).
46. C. Morkel, T. Bodensteiner and H. Gemperlein, *Phys. Rev. E*, **47**, 2575 (1993).
47. D. C. Wallace, *Thermodynamics of Crystals*, (John Wiley and Sons, New York, 1972).